Antimicrobial silver-filled silica nanorattles with low immunotoxicity in dendritic cells

Magdalena Priebe, PhD[a,1], Jérôme Widmer[b,1], Nina Suhartha Löwa, PhD[b],
Sarah-Luise Abram[a], Inès Mottas[b], Anne-Kathrin Woischnig, PhD[c], Priscilla S. Brunetto, PhD[a],
Nina Khanna, PD, MD[c], Carole Bourquin, MD, PhD[b,*,1,2], Katharina M. Fromm, PhD[a,**,1]

[a]*Department of Chemistry, University of Fribourg, Fribourg, Switzerland*
[b]*Department of Medicine, University of Fribourg, Fribourg, Switzerland*
[c]*Department of Biomedicine, University Hospital Basel, Basel, Switzerland*

Abstract

The progression in the use of orthopedic implants has led to an increase in the absolute number of implant infections, triggering a search for more effective antibacterial coatings. Nanorattles have recently gained interest in biomedical applications such as drug delivery, as encapsulation of the cargo inside the hollow structure provides a physical protection from the surrounding environment. Here, silver-containing silica nanorattles ($Ag@SiO_2$) were evaluated for their antimicrobial potential and for their impact on cells of the immune system. We show that $Ag@SiO_2$ nanorattles exhibited a clear antibacterial effect against *Escherichia coli* as well as *Staphylococcus aureus* found in post-operative infections. Immunotoxicological analyses showed that the particles were taken up through an active phagocytic process by dendritic cells of the immune system and did not affect their viability nor induce unwanted immunological effects. Silver-containing silica nanorattles thus fulfill several prerequisites for an antibacterial coating on surgical implants.

Key words: Silver nanoparticles; Silica nanocontainers; Nanorattles; Dendritic cells; Immunoresponse; Antimicrobial properties

*Correspondence to: C. Bourquin, Medicine Department, University of Fribourg, Fribourg, Switzerland.

**Correspondence to: K. Fromm, Chemistry Department, University of Fribourg, Fribourg, Switzerland.

E-mail addresses: carole.bourquin@unifr.ch (C. Bourquin), katharina.fromm@unifr.ch (K.M. Fromm).

[1] These authors contributed equally.

[2] Prof. Dr. Carole Bourquin has moved to University of Geneva: Section of Pharmaceutical Sciences, University of Geneva, Rue Michel-Servet 1, 1211 Geneva, Switzerland.

Each year, a large number of patients undergo joint replacement surgery. Postoperative prosthetic joint infection is a severe complication after arthroplasty that affects 1% to 3% of patients,[1] leading initially to surgical and antibiotic treatment and frequently ending with a need for replacement of the implant.[2,3] It is thus of great importance to develop intelligent nanomaterials which prevent infections and are biocompatible at the same time.[4]

With the emergence of bacterial resistance to conventional antibiotics, silver-based compounds and silver nanoparticles again enjoy rising popularity[5–12] as antimicrobial and healing agents.[13,14] Undoubtedly, the greatest advantage of silver originates from its multidirectional mode of action against microbes. In contrast to single-target antibiotics, the development of resistance is thus more difficult and requires several sequential mutations in the bacterial cell.[14,15] At concentrations within a therapeutic window, silver does not exhibit adverse effects toward mammalian cells while at the same time preventing bacterial survival.[14]

Ag(I)-containing coordination polymers demonstrate good biocompatibility as well as antimicrobial activity, making them promising candidates to fight biomaterial-related infections.[16–18] However, despite their excellent properties, silver is released rapidly during the first weeks after synthesis, leading to a short-term efficacy. For a better controlled, long-term release of silver cations, we propose to use encapsulated silver nanoparticles (AgNPs) as a source of silver cations[19,20] in an inorganic nanocarrier. Nanorattles composed of silica shells may serve as alternatives for silver-based drug delivery because of the possibility of drug loading in their cavity.[21–24] These nanorattles present a strong advantage as they provide a physical barrier for drug protection against the biological environment.[25,26]

Nanoparticles can exhibit immunological effects: particulate material can induce the secretion of proinflammatory cytokines by cells of the immune system[27] or on the contrary suppress immune functions.[28] It is furthermore well established that following arthroplasty, nano-sized debris detach from the implant through wear mechanisms.[29] These debris can interact both locally and systemically with immune cells and induce the release of proinflammatory cytokines such as interleukin-6 (IL-6). In the case of NP designed for biomedical applications such as implant coating, it is therefore critical to carefully assess the impact of particles on the activity of immune cells.

Despite the exceptional antimicrobial properties of AgNPs against bacteria,[30] fungi[31] and viruses,[32] few studies on the preparation of antibacterial nanorattles have been reported so far. Wei et al[33] described Ag@Fe2O3 nanorattles with conjugated glucose. This system serves as an example of multifunctional nanorattles in which glucose captures the bacteria, silver kills them and the magnetic shell allows the efficient removal of the nanorattles from the contaminated drinking water.

Here, we report the synthesis of silica nanorattles filled with silver ($Ag@SiO_2$) made by a microemulsion approach.[34] A first screen to assess whether the $Ag@SiO_2$ particles fulfill a set of requirements in order to be considered for the coating of orthopedic implants was carried out. Antibacterial properties of $Ag@SiO_2$ were tested against both gram-negative and gram-positive bacteria, while the cytotoxicity and the proinflammatory activity were determined with primary immune cells. Additionally, we generated for the first time AgNPs encapsulated inside fluorescent silica shells ($Ag@FITC-SiO_2$) to determine cellular uptake.

Methods

Synthesis of nanocontainers and nanorattles

Non-fluorescent and fluorescent nanorattles were prepared under argon according to the compositions shown in Table S1. First, 1.4 mL of water or $AgNO_3$ (AppliChem, Darmstadt, Germany) aqueous solution (0.01 or 0.05 or 0.1 M) was slowly injected under vigorous stirring into a mixture consisting of 29.6 g of cyclohexane (Sigma-Aldrich, Buchs, Switzerland) and 3.5 mL of Igepal CO-520 (Sigma-Aldrich, Buchs, Switzerland) at 28 °C. After 2 hours, 75 μL of hydrazine monohydrate (Fluka, Buchs, Switzerland) was added and left for 2 hours. Then, silica precursors were added dropwise: first, the non-fluorescent ones

(200 μL of tetraethyl orthosilicate (Sigma-Aldrich, Buchs, Switzerland), 50 μL of 12.5 v/v% ethanolic solution of APTMS) and after 1 hour, the fluorescent one (50 μL of ethanolic solution of FITC-APTMS). After another hour, 500 μL of 28-30% aqueous NH_3 was slowly injected and the reaction was stirred for 36 hours. The microemulsion was destabilized by addition of 25 mL ethanol. The resulting precipitate was collected under centrifugation (15,000 rpm, 30 min, room temperature), washed twice with 25 mL ethanol and 25 mL ultrapure water (15,000 rpm, 15 min, room temperature). Final washing with 20 mL warm ultrapure water (60 °C, 40 min, stirring) followed by centrifugation (15,000 rpm, 15 min, room temperature) resulted in the formation of the void in the silica spheres. Calcination of non-fluorescent NPs was performed during TGA analysis (SDTA/TGA 851^e, Mettler Toledo AG, Greifensee, Switzerland) using aluminum crucibles (40 μL). The measurement was conducted in the presence of nitrogen gas and air to provide combustion of organic residues. The temperature ranged from 25 to 600 °C, with a heating rate of 10 K min^{-1}.

Characterization of nanocontainers and nanorattles

Morphology of the samples is characterized by transmission electron microscopy (TEM) (CM-100 Biotwin Transmission Electron Microscope, FEI/Philips, Hillsboro, Oregon, USA) at the operating voltage of 80 kV, in bright field mode. Sample preparation included a sonication of NPs in ultra-pure water. A drop of diluted suspension was deposited on the TEM grid (Electron Microscopy Sciences, CF 300-Cu, Carbon Film on 300 Square Mesh Copper Grids) and let to dry.

UV–Vis spectra of nanoparticle suspensions were recorded with UV/Vis Spectrometer (Lambda40, Perkin Elmer, Schwerzenbach, Switzerland) at wavelengths ranging from 250 to 800 nm. The fluorescence spectra were measured by using a Luminescence Spectrometer LS 50B (Perkin Elmer, Schwerzenbach, Switzerland) and the Software FL Win Lab. The samples were excited at λ = 492 nm and the spectra were measured within λ = 400-600 nm (Ex. Slit = 5.0, Scan Speed = 100).

Silver loading and release

The amount of silver for each type of nanorattle was determined by ICP after resuspension in nitric acid (32.5%) with ultrasonication. For the silver loading 2-4 mg of $Ag@SiO_2$ nanorattles were suspended in concentrated nitric acid to reach 0.3 mg mL^{-1} and sonicated for about 3 hours before ICP measurements. For silver release analysis 10 mg of $Ag@SiO_2$ nanorattles were resuspended in 5 mL water by vortexing and sonication (30 min). After dilution to a concentration of 0.2 mg mL^{-1} the suspension was split into samples of 1 mL. Those were shaken at 37 °C (200 rpm) in the dark for the required time periods. After centrifugation (2 h, 17,000 rpm) 0.5 mL of the supernatant was taken for ICP analysis. Each time point was analyzed in triplicate.

Spread plate method

$Ag@SiO_2$-3 nanorattles were resuspended in filtrated distilled water and sonicated for 30 minutes. In general, first 100 μL of $Ag@SiO_2$ suspension and then 10^3 to 10^6 cfu mL^{-1} of
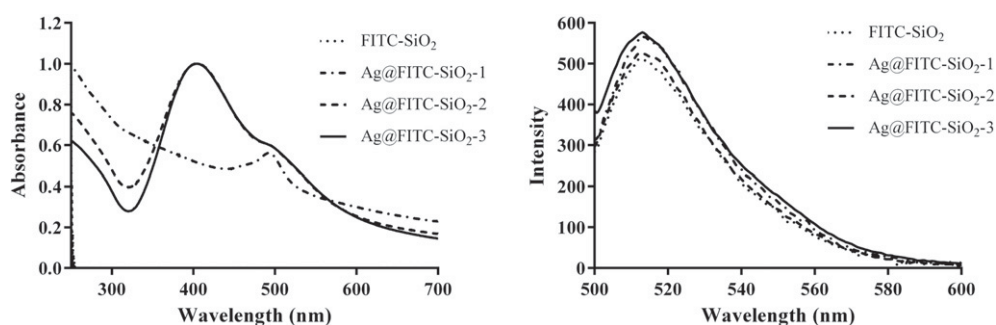
Figure 1. UV–vis spectra (left) and fluorescence spectra (right) of different FITC-SiO$_2$ and Ag@FITC-SiO$_2$ nanorattles. The spectra were normalized.

Escherichia coli (*E. coli.*) K-12 TH14515 suspension was spread on LB agar plates and incubated one day at 37 °C. As negative control, LB agar plates without bacteria and nanorattles were used. The assay was performed in the dark to avoid reduction of possibly present silver cations by light.

Bacterial time-kill study

Glass tubes containing 5 mL trypticase soy broth (TSB; Becton Dickinson and Company, Le Pont de Claix, France) supplemented with either 0.2 mg mL^{-1} or 2 mg mL^{-1} of nanorattles and 5 × 10^6 cfu mL^{-1} of *Staphylococcus aureus* (*S. aureus*)113 wild-type or 1 × 10^6 cfu mL of *E. coli* 25922 were incubated at 37 °C without shaking. Bacterial survival in a silver-free culture and in TSB served as control. Colony counts were determined immediately before addition of silver (0 h) and after 2, 4, 6, 8, and 24 h of incubation with silver at the appropriate concentrations. Before sampling of the probes, the tubes were gently vortexed and colony counts were determined by plating aliquots of appropriate dilutions on Mueller-Hinton agar. A bactericidal effect was defined as a ≥3-log$_{10}$ (≥99.9%) reduction of the initial bacterial count.[35]

Cell viability and stimulation

Bone marrow-derived dendritic cells (BMDC) were prepared as described in supporting information and were resuspended in RPMI1640 (PAA, Pasching, Austria), 2 mmol mL^{-1} L-glutamine (PAA, Glattbrugg, Switzerland), 1 IU mL^{-1} Penicillin (PAA, Pasching, Austria), 100 mg mL^{-1} streptomycin (PAA, Pasching, Austria) with 1% HEPES (PAA, Pasching, Austria), 1 mM sodium pyruvate (PAA, Pasching, Austria), and 50 μM ß-mercaptoethanol (Gibco Life Technologies, provided by Thermo Fisher, Carlsbad, California, United States) supplemented with 10% serum in 96-well plates at a concentration of 10^6 cells mL^{-1}. Nanoparticles were resuspended in pure water, vortexed, then sonicated for 30 min. The suspension (2 mg mL^{-1}) was added directly to the cells to obtain final concentrations from 0.2 μg mL^{-1} to 500 μg mL^{-1}, and cells were then incubated for 24 h at 37 °C under 5% CO$_2$. Each assay was performed in triplicate. 0.2 μg mL^{-1} R848 (Invivogen, Toulouse, France) was used as a positive control for immune activation. After centrifugation of cells (400g, 5 min), supernatants were stored at −20 °C until ELISA analysis. For flow cytometry, cells were resuspended in FACS buffer (PBS, 2.5% bovine serum albumin; BSA, PAA, Pasching, Austria) and

analysis was performed using a MACSQuant Analyzer (Miltenyi Biotec, Bergisch Gladbach, Germany). Propidium iodide was added before measurement. Staurosporine (1 mM) was used as positive control to induce apoptotic cell death. A positive gate was set on CD11c + dendritic cells and data were analyzed using FlowJo software. Interleukin-6 cytokine levels were determined using a commercial kit according to the manufacturer's protocol (Biolegend, London, United Kingdom) and read using a Synergy HT reader (Bio Tek, Luzern, Switzerland).

Nanoparticle uptake

Uptake of FITC-labeled nanoparticles into BMDC was examined by fluorescence microscopy and flow cytometry. BMDC were incubated with Ag@SiO$_2$ nanorattles for 3 h in culture medium (RPMI, 10% FCS, 2 mM L-glutamine, 1 IU mL^{-1} penicillin, 100 μg mL^{-1} streptomycin) at 37 °C in 5% CO$_2$. 75 nM LysoTracker (Invitrogen, provided by Thermo Fisher, Carlsbad, California, United States) and 4′,6-diamidino-2-phenyilindole (DAPI) were used for lysosomal and nuclear staining. Cells were visualized using a fluorescence microscope (Nikon ECLIPSE Ni). In some conditions 10 μM cytochalasin D (Labforce, Muttenz, Switzerland) as phagocytosis inhibitor was added. BMDC were stained with the antibody CD11c-APC-CY7 and with propidium iodide. Cells were then washed twice and examined by flow cytometry (MACSQuant, Miltenyi Biotec, Bergisch Gladbach, Germany).

MTT assay

10^5 BMDC/well were incubated overnight in complete RPMI at 37 °C in the presence of NP. Culture medium was replaced by a medium without phenol red containing clear RPMI Medium 1640 (Gibco Life Technologies, provided by Thermo Fisher, Carlsbad, California, United States), 10% FCS (Gibco Life Technologies, provided by Thermo Fisher, Carlsbad, California, United States), L-glutamine 200 mM (PAA, Pasching, Austria), and 100 IU mL^{-1} Penicillin 100 μg mL^{-1} streptomycin (PAA, Pasching, Austria), to allow photometric assessment. The tetrazolium dye MTT (3-(4,5-dimethylthiazol-2-ul)-2,5-diphenyltetrazolium bromide) (Life Technologies, provided by Thermo Fisher, Carlsbad, California, United States) was added at a final concentration of 1.2 mM and cells were incubated for 4 h at 37 °C. A freshly prepared SDS-HCl solution (10 mL HCl 0.01 M, 1 g SDS) was added and cells were incubated for
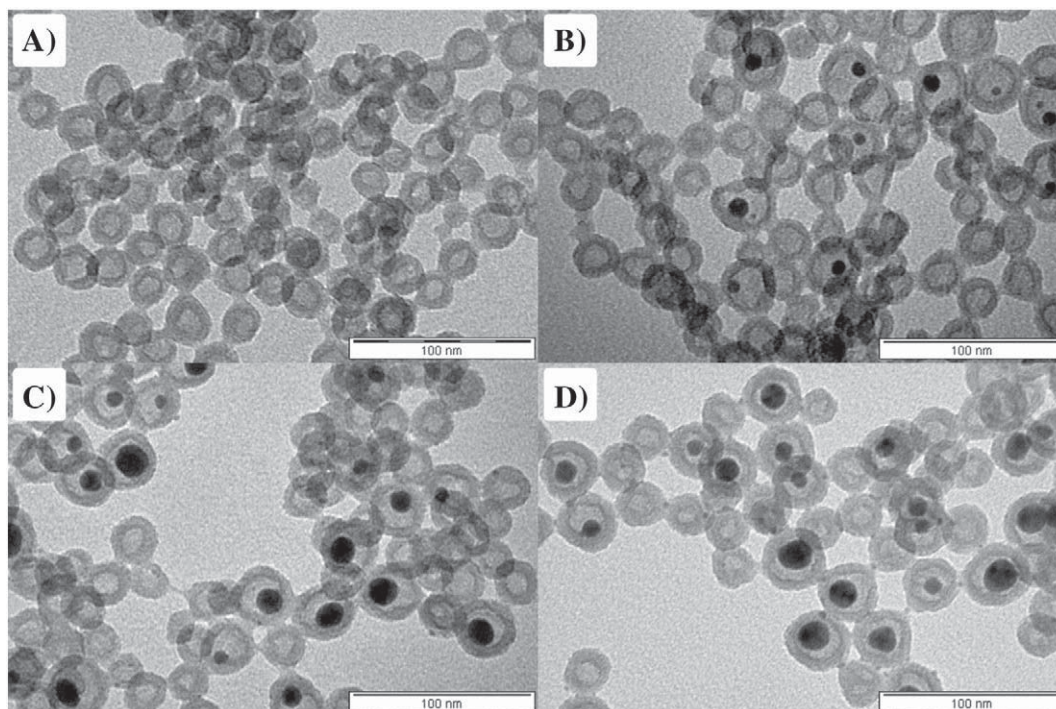
Figure 2. TEM image of as-synthetized **(A)** SiO$_2$, **(B)** Ag@SiO$_2$-1, **(C)** Ag@SiO$_2$-2 and **(D)** Ag@SiO$_2$−3.

a further 4 h. The plate was read at 570 nm using a Synergy HT reader.

Hemolysis assay

Sheep red blood cells (Eurobio, Courtaboeuf, France) were coincubated with 0.2-200 μg mL^{-1} SiO$_2$ or Ag@SiO$_2$ particles in a round bottom 96-well plate in 200 μL PBS at 37 °C, 5% CO$_2$ for 1 h. As positive control for hemolysis, Triton X-100 (Promega, Madison, Wisconsin, United States) was used. 100 μL supernatant was transferred to a flat bottom 96-well plate and read by plate reader (InfinitePro M200, TECAN, Männedorf, Switzerland) at 541 nm. Hemolysis induced by 1% Triton-X was set as 100%.

Results

Preparation and characterization of nanocontainers and nanorattles

SiO$_2$ nanocontainers and Ag@SiO$_2$ nanorattles were synthesized using the water-in-oil microemulsion technique illustrated in Figure S1. The synthesis was performed as previously described.[34] To determine their influence on cells, nanorattles with increasing silver contents were prepared by using 0.01, 0.05 or 0.1 M of AgNO$_3$ aqueous solution during the synthesis, denoted as Ag@SiO$_2$-1, Ag@SiO$_2$-2, Ag@SiO$_2$-3, respectively.

While SiO$_2$ nanocontainers appear colorless, the encapsulation of AgNPs yields suspensions with a color varying from orange to dark brown (Figure S2) depending on the content of silver, size and shape of AgNPs.[36,37] At a low concentration of

AgNPs, their presence can be confirmed exclusively by UV–Vis spectroscopy (Figure S3) due to the large background of the silica shell. Indeed, the prepared Ag@SiO$_2$ nanorattles exhibit a typical surface plasmon band of crystalline spherical AgNP at 410 nm, a typical absorption band for crystalline spherical AgNPs.[38] Higher loading of AgNPs can also be detected by X-ray diffraction (Figure S4).

For tracking the cellular uptake of the nanoparticles, fluorescent nanocontainers (FITC-SiO$_2$) and nanorattles (Ag@FITC-SiO$_2$) were prepared with fluorescein labeling (FITC) (Table S1). Functionalization of the silica shell with a fluorescein derivative leads to chartreuse yellow FITC-SiO$_2$ nanocontainers and dark brown Ag@FITC-SiO$_2$ nanorattles (Figure S2), characterized by UV–Vis (Figure 1). At low silver-loading, the absorption band of the AgNPs is unnoticeable due to the relatively low content of AgNPs compared to FITC (λ_{max} = 494 nm). An increasing filling with silver results in a large band with a maximum at λ_{max} = 405 nm and a small shoulder in the region of the FITC absorption. Since the presence of this small shoulder could potentially originate from larger AgNPs,[36,37,39] fluorescence spectroscopy confirmed the success of functionalization with the fluorescent dye with an FITC emission at λ_{max} = 513 nm (Figure 1). Moreover, FTIR spectra (Figure S5) of both non-fluorescent and fluorescent nanoparticles demonstrated the presence of the silica shell by exhibiting a broad band with a shoulder at 1054 cm^{-1} corresponding to the Si–O–Si siloxane bond vibrations (Figure S5).[40–43]

The transmission electron microscope (TEM) images of the non-fluorescent silica nanocontainers and nanorattles with an increasing content of silver are shown in Figures 2 and 3. In order to study the effect of the surface properties of Ag@SiO$_2$ on
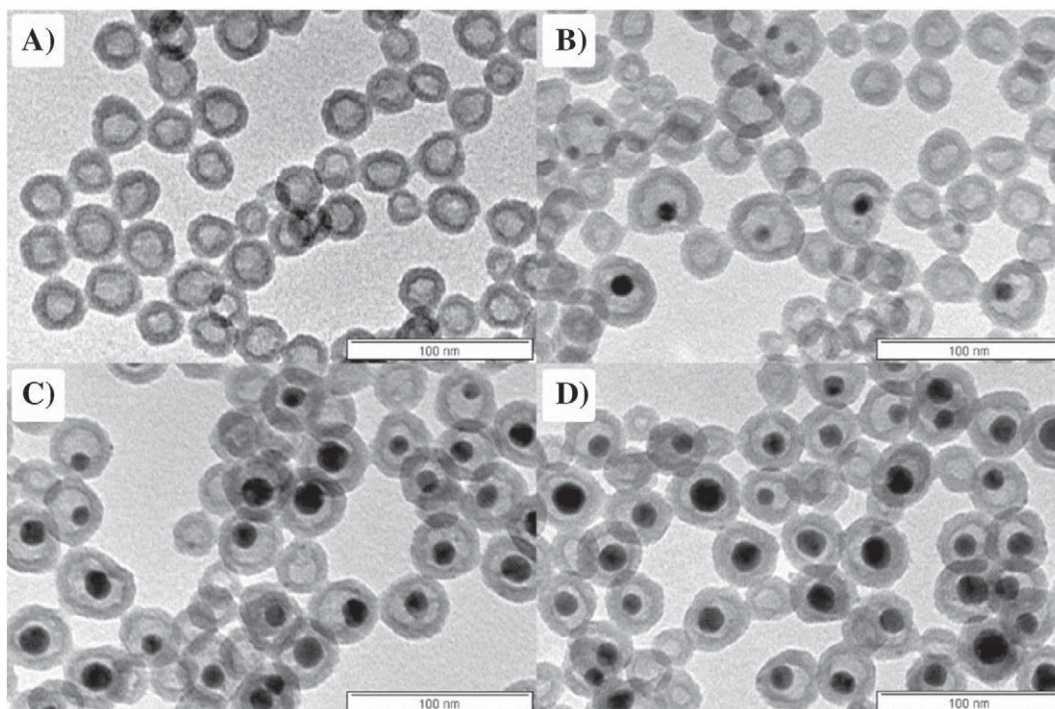
Figure 3. TEM image of **(A)** FITC-SiO$_2$, **(B)** Ag@FITC-SiO$_2$−1, **(C)** Ag@FITC-SiO$_2$−2 and **(D)** Ag@FITC-SiO$_2$-3.

biological assays, calcined Ag@SiO$_2$ rattles were compared to non-calcined ones. Calcination of the above-mentioned Ag@SiO$_2$ does not significantly influence the morphology (Figure S6) even if the NPs are more susceptible to form agglomerates. FITC-SiO$_2$ nanocontainers demonstrate a narrow size distribution with the outer shell diameter ranging from 25 ± 4 nm to 29 ± 6 nm with a wall thickness of 6.2 ± 1.1 nm (Figure S8), which is slightly larger compared to the non-fluorescent SiO$_2$ nanocontainers ranging from 22 ± 4 nm to 25 ± 4 nm with a wall thickness of 5.7 ± 1.4 nm (Figure S7).

Silver loading and release

Under static conditions, the silver release from 3 to 4 µg mL^{-1} for all three Ag@SiO$_2$ samples (Figure S9) is governed by the solubility of the sample in the used medium. This release corresponds to 50% of total silver content for Ag@SiO$_2$-1, 10% for Ag@SiO$_2$-2 and 8% for Ag@SiO$_2$-3 (Figure S10). For further antimicrobial and toxicity investigations, the silver loading of Ag@SiO$_2$ was determined by ICP-OES. The silver content increased with the amount of AgNO$_3$ solutions used during the synthesis from 3.3% for Ag@SiO$_2$-1, 13.4% for Ag@SiO$_2$-2 to 22.8% for Ag@SiO$_2$-3.

Antimicrobial activity of Ag@SiO$_2$ nanorattles

Postoperative prosthetic joint infections are frequently caused by gram-positive cocci, including *S. aureus*, but also by gram-negative bacilli such as *E. coli*. The antibacterial properties of the Ag@SiO$_2$ nanorattles against the model strain, *E. coli* K-12, were analyzed, screening four different bacterial concentrations (10^3-10^6 CFU mL^{-1}) as well as four different concentrations of

Ag@SiO$_2$-3 nanorattles (2.46, 4.67, 9.32, 19.25 mg mL^{-1}). The Ag filled nanorattles demonstrated a concentration- and inoculum-dependent effect and inhibited the bacterial growth of all inocula at their highest concentrations (Figure 4).

The antimicrobial efficacy of the silica nanocontainers and Ag@SiO$_2$ nanorattles was then investigated against gram-positive bacteria *S. aureus* (Figure 5, *E-H*), one of the most virulent strains found in clinic for biomaterial related infections,[3] and compared to *E. coli* strains (Figure 5 *A-D*). After being incubated with bacterial cultures at 37 °C for different time intervals, two different concentrations (0.2 and 2 mg mL^{-1}) of SiO$_2$ hollow spheres (negative controls) as well as Ag@SiO$_2$ nanorattles with increasing concentrations of AgNO$_3$ (0.01 M, 0.05 M and 0.1 M) were assessed. As shown in Figure 5, silica hollow spheres did not inhibit the growth of both *E. coli* and *S. aureus*, while Ag@SiO$_2$ nanorattles showed an increasing inhibitory activity when an increasing amount of silver precursor was used. Silver has a stronger effect against gram-negative bacteria (Figure 5 *A-D*) than for gram-positive bacteria (Figure 5 *E-H*). After 24 h, no antibacterial effect was observed with Ag@SiO$_2$-1 (Figure 5, *F*) and Ag@SiO$_2$-2 (Figure 5, *G*) for *S. aureus* while only 2 mg mL^{-1} of AgSiO$_2$-3 (Figure 5, *H*) showed a decrease of around 3 log.

Uptake of SiO$_2$ nanocontainers into immune cells

To assess the uptake of NPs into immune cells, primary cultures of murine bone marrow-derived dendritic cells (BMDC) were used. Dendritic cells are cells of the immune system that are highly specialized in the uptake of particulate material and in the initiation of immune responses against infectious pathogens. BMDC were incubated for 3 to 4 h with fluorescently labeled FITC-Ag@SiO2 nanoparticles and uptake was determined by
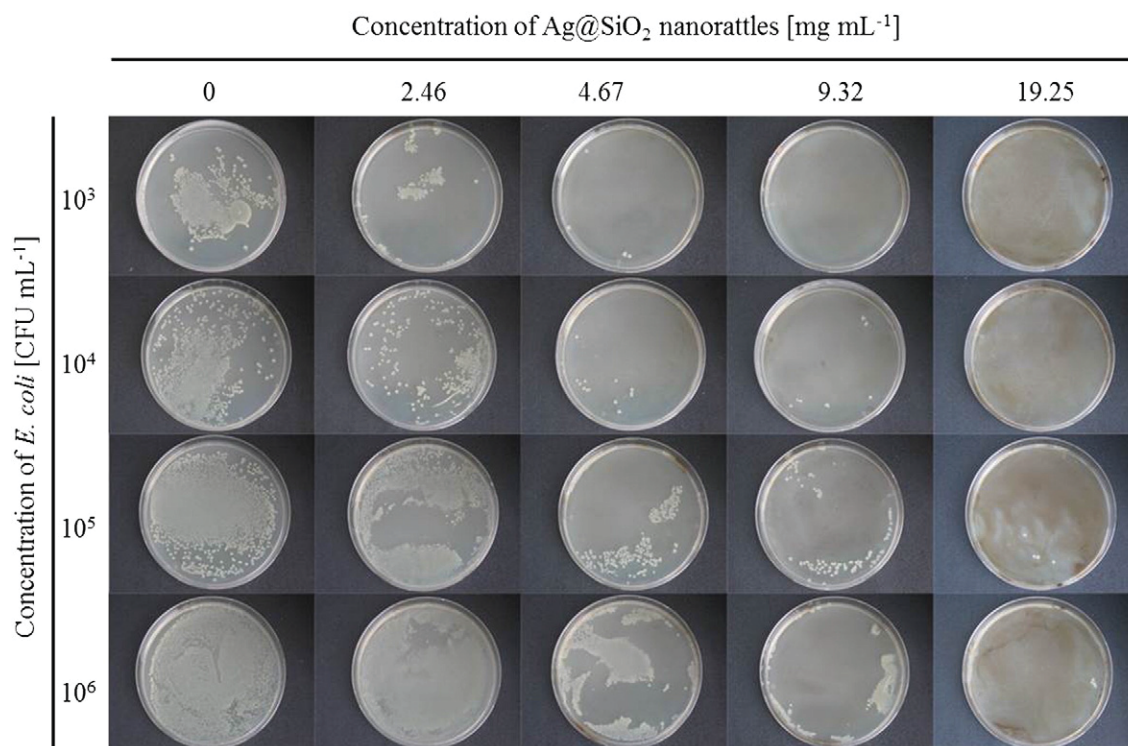
Figure 4. Digital images of agar plates demonstrating antimicrobial properties of Ag@SiO$_2$-3 nanorattles against *E. coli* K-12 using the spread plate method.

flow cytometry. As shown in Figure 6, *A*, cells incubated with fluorescent nanocontainers at 37 °C demonstrate high FITC fluorescence compared to cells incubated without nanocontainers. We assessed whether the uptake of the nanoparticles was an active process by incubating BMDC with FITC-Ag@SiO2 on ice. Low temperatures inhibit biological processes and have been shown to block the internalization of NPs.[44] The increase in fluorescence was largely blocked by incubation of the cells on ice, suggesting that FITC-Ag@SiO2 uptake into BMDC is an active biological process. The slight increase in fluorescence seen in cells incubated with NPs on ice compared to cells without NPs suggested that a small amount of nanocontainers adhere passively to the cell surface.

To further characterize the uptake mechanism and verify whether silver-containing SiO$_2$ nanorattles were also taken up by BMDC, we co-incubated BMDC and Ag@FITC-SiO$_2$-3 nanorattles at two different concentrations for 3 h in the presence of cytochalasin D, a phagocytosis inhibitor that inhibits the actin-dependent uptake of NP.[45] Uptake of the nanorattles is clearly demonstrated by the concentration-dependent increase in FITC fluorescence of BMDC (Figure 6, *B*). Incubation with cytochalasin D completely blocked Ag@FITC-SiO$_2$-3 uptake, indicating that the particles are internalized by a phagocytic process. The intracellular localization of the particles was then examined by microscopy. As depicted in Figure 6, *C* and *D*, fluorescence microscopy showed the colocalization (yellow) of green Ag@FITC-SiO2 (Figure 6, *C*) and Ag@FITC-SiO2 (Figure 6, *D*) with the endosomal marker LysoTracker (red),

demonstrating that the NPs are concentrated in endosomal vesicles in dendritic cells.

Impact of SiO$_2$ particles on cellular and immunological function

To assess whether SiO$_2$ and Ag@SiO$_2$ particles exhibit toxicity on BMDC, we incubated BMDC with increasing concentrations of particles for 24 h. Viability of cells was measured by propidium iodide incorporation. As shown in Figure 7, *A*, we detected no significant decrease in cell survival after treatment with Ag-free SiO$_2$ particles, even at the highest particle concentration of 200 µg mL^{-1}. A decrease in viability was observed in BMDC treated with Ag@SiO2 only at very high concentrations. In terms of experimental procedure, the Ag@SiO2 were resuspended in water and directly added to the cell culture. Since no pre-treatment of specimens was necessary, encapsulation of AgNPs inside silica nanocontainers seems to provide a sufficient protection from the initial release of silver cations, at least up to concentrations of 20 µg mL^{-1} AgNPs. We also measured the hemolytic activity of SiO$_2$ and Ag@SiO2. Only the highest concentration of 200 µg mL^{-1} induced moderate hemolysis (Figure 7, *B*).

Since Ag@SiO$_2$ nanorattles only affected cell viability at high concentrations, the next step was to verify whether these nanorattles immunologically activate BMDC. The secretion of the proinflammatory cytokine interleukin 6 (IL-6) was used as a sensitive assessment of BMDC activation. As positive control, BMDC were stimulated with resiquimod (R848), which is
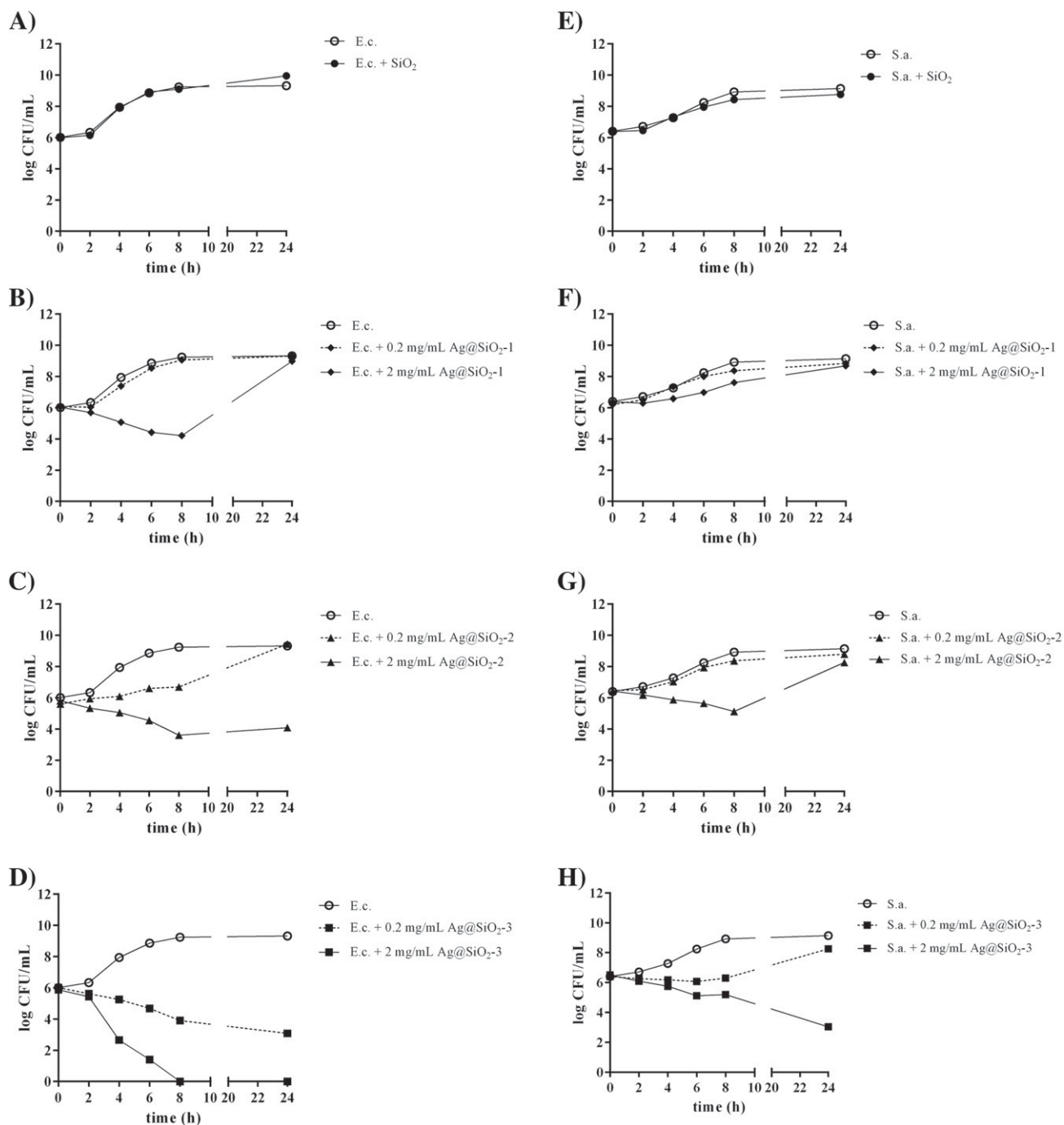
Figure 5. Killing curves of *E. coli* (from A to D) and *S. aureus* (from E to H) at two concentrations of **(A** and **E)** SiO$_2$, **(B** and **F)** Ag@SiO$_2$-1, **(C** and **G)** Ag@SiO$_2$-2 and **(D** and **H)** Ag@SiO$_2$-3.

known to activate immune cells and stimulate IL-6 production.[46] Ag@SiO$_2$ nanorattles did not induce IL-6 production at concentrations ranging from 2 to 500 µg mL^{-1} (data not shown). We then examined whether nanocontainers and nanorattles impact cytokine production induced by R848. We observed that Ag-free silica nanocontainers did not inhibit R848-induced IL-6 secretion at concentrations up to 20 µg mL^{-1} (Figure 8, *A*). At the highest concentration of 200 µg mL^{-1}, nanocontainers inhibited IL-6 production by approximately

50%. The impact of as-synthesized and calcined Ag@SiO$_2$ nanorattles containing increasing amounts of silver was also examined. We observed that as-synthesized nanorattles inhibited IL-6 production only at the highest NP concentration of 200 µg mL^{-1}. In contrast, calcined Ag@SiO$_2$ nanorattles already inhibited IL-6 production at 20 µg mL^{-1} with 0.1 M Ag (Ag@SiO$_2$-3) and even blocked IL-6 production entirely at 200 µg mL^{-1} with 0.1 M Ag. In summary, we show two different effects on IL-6 secretion: a) Ag@SiO$_2$ nanorattles inhibit IL-6
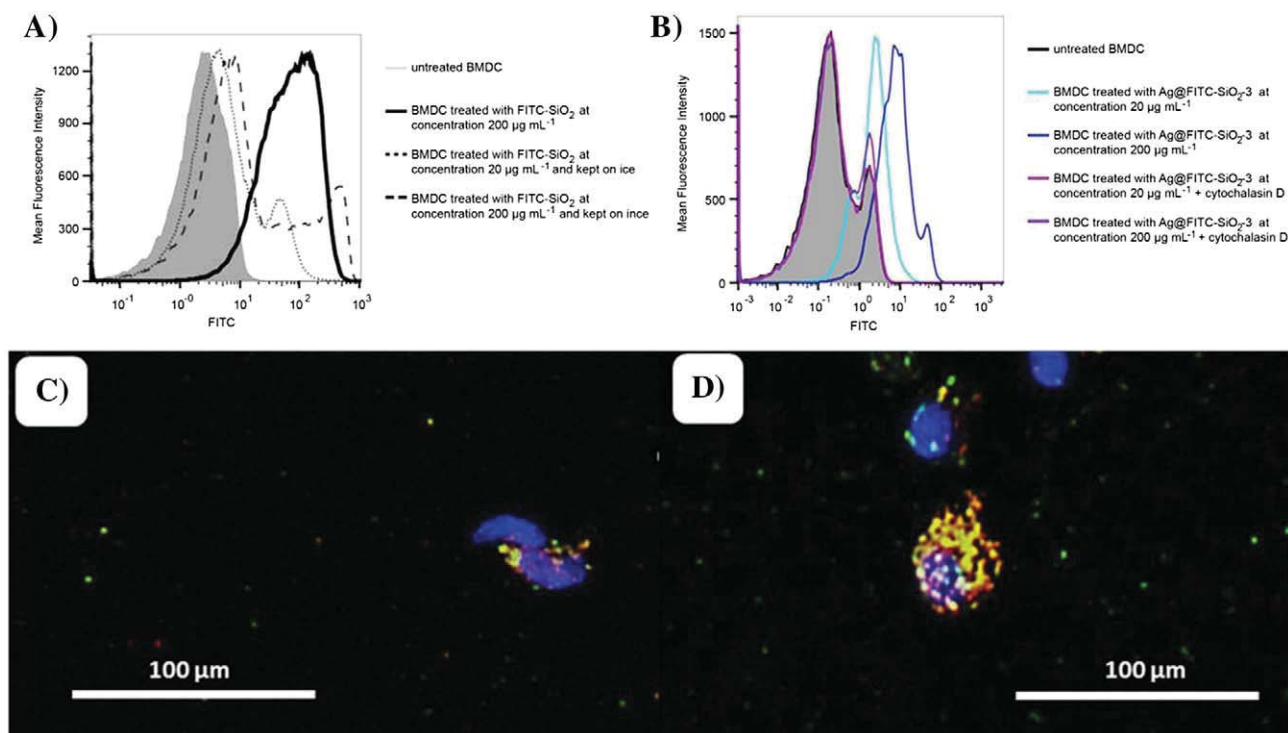
Figure 6. Uptake of FITC-SiO$_2$ nanocontainers by BMDC. (**A** and **B**) BMDC were incubated for 3 h with FITC-labeled Ag@SiO2 and uptake by CD11c$^+$ BMDC was assessed by flow cytometry. (**C** and **D**) Fluorescent micrographs of BMDC incubated for 3 h with 50 µg mL^{-1} FITC-labeled Ag@SiO2 (**C**) or FITC-labeled Ag@SiO2 containing 0.1 M AgNO$_3$ (**D**). Green: FITC-labeled nanoparticles, red: lysoTracker (endosomal marker), blue: cell nuclei (DAPI). Yellow: merged green and red.

production at high Ag loadings, and b) calcined NPs containing high loadings of Ag inhibit IL-6 production more than non-calcined NPs.

To examine whether the immune function of BMDC was selectively inhibited by Ag@SiO$_2$ or whether other cellular functions were also affected, we performed an MTT assay to measure cellular metabolic activity due to NAD(P)H flux. We show that metabolic activity was only moderately decreased at NP concentrations of 2 and 20 µg mL^{-1} with or without Ag, but was nearly entirely blocked at the highest NP concentration of 200 µg mL^{-1} in the presence of Ag (Figure 8, *B*). Thus, Ag@SiO2 at the highest concentration impaired BMDC metabolism.

Discussion

In the current study we examined whether Ag-filled nanorattles fulfill a set of essential criteria in order to be considered for the antibacterial coating of orthopedic implants.

SiO$_2$, Ag@SiO$_2$, FITC-SiO$_2$ and Ag@FITC-SiO$_2$ nanocontainers used in this study were first synthetized via the water-in-oil microemulsion approach[35] and characterized. By varying different experimental parameters (Table S1) such as the concentration of silver nitrate solution during the synthesis, the extent of loading of the Ag@SiO2 could be tuned. The AgNP presence was confirmed by UV–Vis analysis with a surface plasmon band at 410 nm (Figure S3), a typical absorption band for crystalline spherical AgNPs.[38] Dynamic light scattering

(DLS) analysis revealed a small zeta potential of all nanorattles (Table S2), indicating a low colloidal stability and a tendency to agglomerate in aqueous suspensions. TEM results showed that calcination process does not influence the morphology of the Ag@SiO$_2$ nanorattles (Figure S6). Filling of nanocontainers with AgNPs results in an enlargement of the nanocontainers to a maximum of 29 nm, while increasing the concentration of AgNO$_3$ from 0.01 M, 0.05 M to 0.1 M allows tuning of the AgNPs size (10.5 ± 2.2 nm, 14.3 ± 2.6 nm and 16.4 ± 3.8 nm, respectively).

The antimicrobial activity of the Ag@SiO$_2$ nanorattles was investigated against two types of bacteria that are frequently involved in infectious complications of orthopedic implants, the gram-positive *S. aureus* and the gram-negative *E. coli*. Indeed, *S. aureus* causes more than 50% of all implant-associated infections.[3,47–49] Gram-negative bacteria are more sensitive against Ag@SiO$_2$ than gram-positive bacteria, also demonstrated by Klapiszewski and co-workers[50] The comparison of the antimicrobial efficacy of silica nanorattles with different silver loadings (Figure 5) shows a clear supremacy of the nanorattles with higher silver loading. Indeed the bacterial growth was inhibited when the concentration of Ag@SiO$_2$ increased to 2 mg mL^{-1}. Ag@SiO$_2$ Nanorattles demonstrated a typical dose-dependent effect against *E.coli* strains. This is in agreement with previous studies of Das et al,[51] and Parandhaman et al,[52] in which nano-silica silver composites exhibited antibacterial activities with 99.9% killing effect. The dose-dependency can be explained by the continuous uptake of silver by the bacteria,
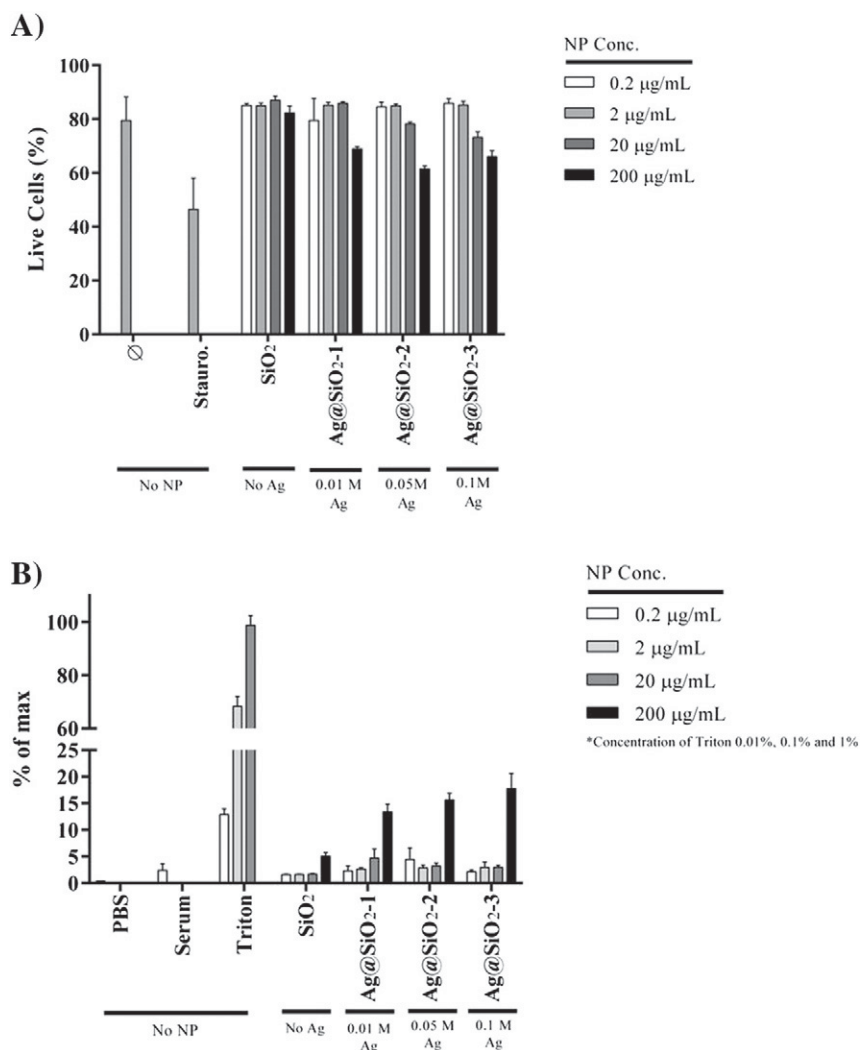
Figure 7. Effect of SiO$_2$ nanocontainers and Ag@SiO$_2$ nanorattles on BMDC and red blood cell viability. BMDC were treated with increasing concentrations of SiO$_2$ hollow spheres or Ag@SiO$_2$ nanorattles containing increasing concentrations of AgNO$_3$. **(A)** Viability was measured by propidium iodide incorporation into CD11c$^+$ cells. **(B)** Sheep red blood cells were incubated for 1 h with increasing concentrations of nanoparticles. Absorbance of supernatant was measured at 541 nm.

which leads to a non-static, hence continuous release of silver from the nanorattle reservoirs until bacteria are killed. This is realized with the highest loaded nanocontainers.

We have studied the interaction of Ag@SiO$_2$ with mouse dendritic cells, which play an essential role in the initiation and control of immune responses. These cells are able to phagocytose particulate bodies and, upon activation, to produce high amounts of cytokines, which are essential messengers of immunity.[53–55] Indeed, dendritic cells are key regulators of both immune tolerance and antimicrobial immunity. The study of the impact of NP on the function of dendritic cells is therefore of utmost importance for future clinical applications.

According to their size and morphology, nanoparticles can be internalized into cells by either passive or active pathways.[56] Since the majority of the SiO$_2$ nanocontainers does not exceed 30 nm in diameter, their uptake can be expected to follow the endocytic pathway.[57] However, as it was demonstrated by TEM images and confirmed by DLS measurements, the silica shells tend to form

agglomerates which could modify the cellular uptake. We demonstrate here that Ag@SiO$_2$ nanorattles are actively taken up by dendritic cells in an actin-dependent process and can subsequently be found in the endosome, suggesting an uptake by phagocytosis.

It is known that the NP surface becomes coated with biomolecules present in biological fluids in a phenomenon called the corona. The composition of the corona is dependent on the environment and can influence NP uptake in certain cell types.[58] In our study, the cellular uptake experiments were performed in standard cell culture medium containing 10% fetal calf serum, which differs from physiological conditions found in the organism. Thus, although dendritic cells are well known to take up many different types of NP,[58] it will be important to verify uptake of Ag@SiO$_2$ NPs by dendritic cells in future in vivo studies.

The cytotoxicity of nanomaterials is clearly size-dependent.[59] Choi et al showed, for example, that silicon nanoparticles are more cytotoxic than larger silicon microspheres due to
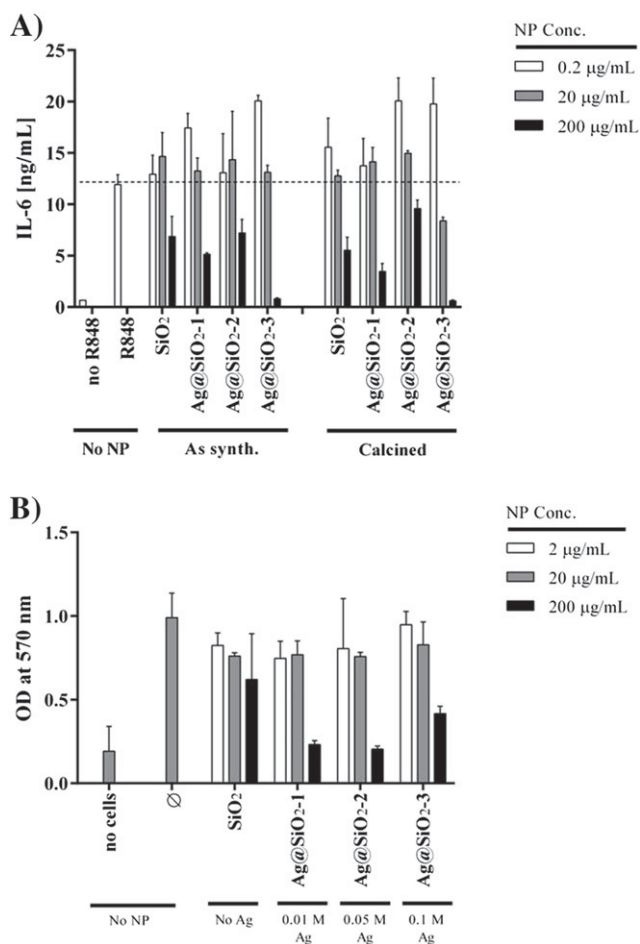
Figure 8. Effect of SiO$_2$ and Ag@SiO$_2$ nanoparticles on BMDC function. BMDC were incubated for 24 h with increasing concentration of Ag@SiO$_2$ nanoparticles. After 4 h incubation, cells were stimulated by the addition of 0.2 μg mL^{-1} R848 and incubated for a further 20 h. **(A)** IL-6 production was assessed by ELISA of supernatants. **(B)** NAD(P)H-dependent metabolism was measured by MTT assay.

differences in the specific surface area, the number of particles at the equivalent gram concentration and the internalization pathway.[60] The cytotoxicity of silver is highly dependent on its concentration: within a defined therapeutic window it has antimicrobial properties but does not affect mammalian cells, making it an effective antibacterial agent.[14] We show here that neither SiO$_2$ nanocontainers nor Ag@SiO$_2$ nanorattles affect the viability of dendritic cells except at the highest concentrations. The highest concentrations of Ag@SiO$_2$ nanorattles (200 μg mL^{-1}) also impair dendritic cell metabolism measured by MTT assay.

Some nanoparticles such as nano-TiO$_2$ have been shown to activate BMDC and other immune cell subsets to produce proinflammatory cytokines.[27] This activation occurs through the NLRP3 inflammasome, a cytosolic protein complex. Such a proinflammatory activity would be highly undesirable in materials used for coating surgical implants, as this might result in chronic inflammation at the site of the implant, which could compromise its integrity and function. We have observed here

that Ag@SiO$_2$ nanorattles do not induce the proinflammatory cytokine IL-6, even at high concentrations of NP. Thus, we show that dendritic cells readily phagocyte Ag@SiO$_2$ NP but that in contrast to the uptake of TiO$_2$ NP, they are not activated following internalization.

While the materials coating implants should not spontaneously induce inflammation, these materials should not inhibit the activity of local immune cells. We have mimicked the initiation of an immune response by using R848, an activator of the Toll-like receptor 7. This molecule initiates a strong immune response in dendritic cells by inducing the production of cytokines. We have demonstrated that as-synthesized Ag@SiO$_2$ nanorattles do not impair immune activation of BMDC upon R848 stimulation for concentrations up to 20 μg mL^{-1} NP and 0.1 M AgNO$_3$. Under the same conditions, calcinated nanorattles do decrease the production of IL-6 in an Ag concentration-dependent manner.

In conclusion, we have demonstrated that silica-encapsulated Ag has strong antibacterial properties at a concentration that is neither hemolytic nor affects the viability of phagocytic cells. Furthermore, Ag@SiO$_2$ NPs did not induce inflammation and did not impair immune responses at this concentration. As it is clear that nanoparticulate debris are released by wear in the case of orthopedic implants, and that these debris are taken up by dendritic cells and other immune cells, it was essential to clarify the absence of toxicity and of adverse effects on the immune system for Ag@SiO$_2$ NPs in particulate form. In further studies, it will be necessary to confirm the antibacterial effect of Ag@SiO$_2$ NPs when immobilized as coating on implant material. Thus, we have shown that Ag@SiO$_2$ NPs fulfill important prerequisites for their application as antibacterial coating of surgical implants.

Appendix A. Supplementary data

Supplementary data to this article can be found online at http://dx.doi.org/10.1016/j.nano.2016.08.002.

References

1. Pavithra D, Doble M. Biofilm formation, bacterial adhesion and host response on polymeric implants-issues and prevention. *Biomed Mater* 2008;**3**:034003.
2. Pye A, Lockhart D, Dawson M, Murray C, Smith A. A review of dental implants and infection. *J Hosp Infect* 2009;**72**:104-10.
3. Nishimura S, Tsurumoto T, Yonekura A, Adachi K, Shindo H. Antimicrobial susceptibility of *Staphylococcus aureus* and *Staphylococcus epidermidis* biofilms isolated from infected total hip arthroplasty cases. *J Orthop Sci* 2006;**11**:46-50.
4. Bruellhoff K, Fiedler J, Möller M, Groll J, Brenner RE. Surface coating strategies to prevent biofilm formation on implant surfaces. *Artif Organs* 2010;**33**:646-53.
5. Chopra I. The increasing use of silver-based products as antimicrobial agents: a useful development or a cause for concern? *J Antimicrob Chemother* 2007;**59**:587-90.
6. Chaloupka K, Malam Y, Seifalian AM. Nanosilver as a new generation of nanoproduct in biomedical application. *Trends Biotechnol* 2010;**28**:580-8.

7. Strydom SJ, Rose WE, Otto DP, Liebenberg W, de Villiers MM. Poly(amidoamine) dendrimer-mediated synthesis and stabilization of silver sulfonamide nanoparticles with increased antibacterial activity. *Nanomedicine: NBM* 2013;**9**:85-93.

8. Martinez-Gutierrez F, Olive PL, Banuelos A, Orrantia E, Nino N, Morales Sanchez E, Ruiz F, Bach H, Av-Gay Y. Synthesis, characterization, and evaluation of antimicrobial and cytotoxic effect of silver and titanium nanoparticle. *Nanomedicine: NBM* 2010;**2010**(6):681-8.

9. Svensson S, Suska F, Emanuelsson L, Palmquist A, Norlindh B, Trobos M, Bäckros H, Persson L, Rydja G, Ohrlander M, Lyvén B, Lausmaa J, Thomsen P. Osseointegration of titanium with an antimicrobial nanostructured noble metal coating. *Nanomedicine: NBM* 2013;**9**:1048-56.

10. Mohanty S, Mishra S, Jena P, Jacob B, Sarkar B, Sonawane A. An investigation of the antibacterial, cytotoxic, and antibiofilm efficacy of starch-stabilized silver nanoparticles. *Nanomedicine: NBM* 2012;**8**:916-24.

11. Cavaliere E, de Cesari S, Landini G, Riccobono E, Pallecchi L, Rossolini GM, Gavioli L. Highly bacterial Ag nanoparticle films obtained by cluster beam deposition. *Nanomedicine* 2015;**11**:1417-23.

12. Brandt O, Mildner M, Egger AE, Groessl M, Rix U, Posch M, Keppler BK, Strupp C, Mueller B, Stingl G. Nanoscalic silver possesses broad-spectrum antimicrobial activities and exhibits fewer toxicological side effects than silver silfadiazine. *Nanomedicine* 2012;**8**:478-88.

13. Chernousova S, Epple M. Silver as antibacterial agent: ion, nanoparticle, and metal. *Angew Chem Int Ed* 2013;**52**:1636-53.

14. Eckhardt S, Brunetto PS, Gagnon J, Priebe M, Giese B, Fromm KM. Nanobio silver: its interactions with peptides and bacteria, and its uses in medicine. *Chem Rev* 2013;**113**:4708-54.

15. Spratt B. Resistance to antibiotics mediated by target alterations. *Science* 1994;**264**:388-93.

16. Vig Slenters T, Hauser-Gerspach I, Daniels AU, Fromm KM. Silver coordination compounds as light-stable, nano-structured and anti-bacterial coatings for dental implant and restorative materials. *J Mater Chem* 2008;**18**:5359-62.

17. Gordon O, Vig Slenters T, Brunetto PS, Villaruz AE, Sturdevant DE, Otto M, Landmann R, Fromm KM. Silver coordination polymers for prevention of implant infection: thiol interaction, impact on respiratory chain enzymes, and hydroxyl radical induction. *Antimicrob Agents Chemother* 2010;**54**:4208-18.

18. Brunetto PS, Vig Slenters T, Fromm KM. In vitro biocompatibility of new silver (I) coordination compound coated surfaces for dental implant applications. *Materials* 2011;**4**:355-67.

19. Kittler S, Greulich C, Diendorf J, Köller M, Epple M. Toxicity of silver nanoparticles increases during storage because of slow dissolution under release of silver ions. *Chem Mater* 2010;**22**:4548-54.

20. Zhang W, Yao Y, Sullivan N, Chen Y. Modeling the primary size effects of citrate-coated silver nanoparticles on their ion release kinetics. *Environ Sci Technol* 2011;**45**:4422-8.

21. Song G, Li C, Hu J, Zou R, Xu K, Han L, Wang Q, Yang J, Chen Z, Qin Z, Ruan K, Hu R. A simple transformation from silica core-shell-shell to yolk-shell nanostructures: a useful platform for effective cell imaging and drug delivery. *J Mater Chem* 2012;**22**:17011-8.

22. Liu B, Wang J, Sun S, Wang X, Zhao M, Zhang W, Zhang H, Yang X. A general method for the synthesis of various rattle-type microspheres and their diverse applications. *RSC Adv* 2013;**3**:18506-18.

23. Zhu Y, Kockrick E, Ikoma T, Hanagata N, Kastel S. An efficient route to rattle-type Fe$_3$O$_4$@SiO$_2$ hollow mesoporous spheres using colloidal carbon spheres templates. *Chem Mater* 2009;**21**:2547-53.

24. Sekhon BS, Kamboj SR. Inorganic nanomedicine – part 2. *Nanomedicine: NBM* 2010;**6**:612-8.

25. Wu SH, Tseng CT, Lin YS, Lin CH, Hung Y, Mou CY. Catalytic nanorattle of Au@hollow silica: towards a poison-resistant nanocatalyst. *J Mater Chem* 2010;**21**:789-94.

26. Sun Y, Duan L, Guo Z, DuanMu Y, Ma M, Xu L, Zhang Y, Gu N. An improved way to prepare superparamagnetic magnetite-silica core-shell nanoparticles for possible biological application. *J Magn Mater* 2005;**285**:65-70.

27. Yazdi AS, Guarda G, Riteau N, Drexler SK, Tardivel A, Couillin I, Tschopp J. Nanoparticles activate the NLR pyrin domain containing 3 (Nlrp3) inflammasome and cause pulmonary inflammation through release of IL-1α and IL-1β. *PNAS* 2010;**107**:19449-54.

28. Vandebriel RJ, Tonk ECM, de la Fonteyne-Blankestijn LJ, Gremmer ER, Verharen HW, van der Ven LT, van Loveren H, de Jong WH. Immunotoxicity of silver nanoparticles in an intravenous 28-day repeated-dose toxicity study in rats. *Part Fibre Toxicol* 2014;**11**:21.

29. Hosman AH, van der Mei HC, Bulstra SK, Busscher HJ, Neut D. Effects of metal-on-metal wear on the host immune system and infection in hip arthroplasty. *Acta Orthop* 2010;**81**:526-34.

30. Guzman M, Dille J, Godet S. Synthesis and antibacterial activity of silver nanoparticles against gram-positive and gram-negative bacteria. *Nanomedicine* 2012;**8**:35-45.

31. Kim SW, Jung JH, Lamsal K, Kim YS, Min JS, Lee YS. Antifungal effects of silver nanoparticles (AgNPs) against various plant pathogenic fungi. *Myconet* 2012;**40**:53-8.

32. Xiang DX, Chen Q, Pang L, Zheng CL. Inhibition of A/Human/Hubei/3/2005 (H3N2) influenza virus infection by silver nanoparticles in vitro and in vivo. *J Virol Methods* 2011;**178**:137-42.

33. Wei Z, Zhou Z, Yang M, Lin C, Zhao Z, Huang D, Chen Z, Gao J. Multifunctional Ag@Fe$_2$O$_3$ yolk-shell nanoparticles for simultaneous capture, kill, and removal of pathogen. *J Mater Chem* 2011;**21**:16344-8.

34. Priebe M, Fromm KM. One-pot synthesis and catalytic properties of encapsulated silver nanoparticles in silica nanocontainers. *Part Syst Character* 2014;**31**:645-51.

35. National Committee for Clinical Laboratory Standards. Methods for determining bactericidal activity of antimicrobial agents. *NCCLS Document M26-A*. National Committee for Clinical Laboratory Standards V: PA; 1999.

36. Jin R, Cao YW, Mirkin CA, Kelly KL, Schatz GC, Zheng JG. Photoinduced conversion of silver Nanospheres to Nanoprisms. *Science* 2001;**294**:1901-3.

37. Lee MH, Oh SG, Suh KD, Kim DG, Sohn D. Preparation of silver nanoparticles in hexagonal phase formed by nonionic Triton X-100 surfactant. *Physicochem Eng Asp* 2002;**210**:49-60.

38. Shirtcliffe N, Nicle U, Schneider S. Reproducible preparation of silver sols with small particle size using borohydride reduction: for use as nuclei for preparation of larger particles. *J Colloid Interface Sci* 1999;**211**:122-9.

39. van Hyning DL, Zukoski C. Formation mechanisms and aggregation behavior of borohydride reduced silver particles. *Langmuir* 1998;**14**:7034-46.

40. Zeng T, Zhang X, Ma Y, Wang S, Niu H, Cai Y. A functional rattle-type microsphere with a magnetic-carbon double-layered shell for enhanced extraction of organic targets. *Chem Commun* 2013;**49**:6039-41.

41. Yan N, Chen Q, Wang F, Wang Y, Zhong H, Hu L. High catalytic activity for CO oxidation of Co$_3$O$_4$ nanoparticles in SiO$_2$ nanocapsules. *J Mater Chem A* 2012;**1**:637-43.

42. Liu A, Wu L, He Z, Zhou J. Development of highly fluorescent silica nanoparticles chemically doped with organic dye for sensitive DNA microarray detection. *Anal Bioanal Chem* 2011;**401**:2003-11.

43. Yamaura M, Camilo R, Sampaio L, Macêdo M, Nakamura M, Toma H. Preparation and characterization of (3-aminopropyl) triethoxysilane-coated magnetite nanoparticles. *J Magn Mater* 2004;**279**:210-7.

44. Sokolova V, Kozlova D, Knuschke T, Buer J, Westendorf AM, Epple M. Mechanism of the uptake of cationic and anionic calcium phosphate nanoparticles by cells. *Acta Biomater* 2013;**9**:7527-35.

45. Karlson TDL, Kong YY, Hardy CL, Xiang SD, Plebanski M. The signalling imprints of nanoparticle uptake by bone marrow derived dendritic cells. *Methods* 2013;**60**:275-83.

46. Ahonen CL, Gibson SJ, Smith RM, Pederson LK, Lindh JM, Tomai MA, Vasilakos JP. Dendritic cell maturation and subsequent enhanced T-cell stimulation induced with the novel synthetic immune response modifier R-848. *Cell Immunol* 1999;**197**:62-72.

47. Rosenthal KS, Tan MJ. *Rapid review microbiology and immunology.* Philadelphia, PA: Mosby/Elsevier; 2011.

48. Schierholz J, Beuth J. Implant infections: a haven for opportunistic bacteria. *J Hosp Infect* 2001;**49**:87-93.

49. Campoccia D, Montanaro L, Arciola CR. A review of the biomaterials technologies for infection-resistant surfaces. *Biomaterials* 2013;**34**:8533-54.

50. Klapiszewski L, Rzemieniecki T, Krawczyk M, Malina D, Norman M, Zdarta J, Majchrzak I, Dobrowolska A, Czaczyk K, Jesionowski T. Kraft lignin/silica-AgNPs as a functional material with antimicrobial activity. *Colloids Surf B: Biointerfaces* 2015;**134**:220-8.

51. Das SK, Khan MR, Parandhaman T, Laffir F, Guha AK, Sekaran G, Mandal SB. Nano-silica fabricated with silver nanoparticles: antifouling adsorbent for efficient dye removal, effective water disinfection and biofouling control. *Nanoscale* 2013;**5**:5549-60.

52. Parandhaman T, Das A, Ramalingam B, Samanta D, Sastry TP, Mandal AB, Das SK. Antimicrobial behavior of biosynthesis silica-silver nanocomposite for water disinfection: a mechanistic perspective. *J Hazard Mater* 2015;**290**:117-26.

53. Schüller VJ, Heidegger S, Sandholzer N, Nickels PC, Suhartha NA, Endres S, Bourquin C, Liedl T. Cellular Immunostimulation by CpG-sequence-coated DNA origami structures. *ACS Nano* 2011;**5**:9696-702.

54. Heidegger S, Kirchner SK, Stephan N, Bohn B, Suhartha N, Hotz C, Anz D, Sandholzer N, Stecher B, Russmann H, Endres S, Bourquin C. TLR activation excludes circulating naive CD8+ T cells from gut-associated lymphoid organs in mice. *J Immunol* 2013;**190**:5313-20.

55. Bourquin C, von der Borch P, Zoglmeier C, Anz D, Sandholzer N, Suhartha N, Wurzenberger C, Denzel A, Kammerer R, Zimmermann W, Endres S. Efficient eradication of subcutaneous but not of autochthonous gastric tumors by adoptive T cell transfer in an SV40 T antigen mouse model. *J Immunol* 2010;**185**:2580-8.

56. Li WR, Xie XB, Shi QS, Zeng HY, Ou-Yang YS, Chen YB. Antibacterial activity and mechanism of silver nanoparticles on *Escherichia coli*. *Appl Microbiol Biotechnol* 2010;**85**:1115-22.

57. Petros RA, DeSimone JM. Strategies in the design of nanoparticles for therapeutic applications. *Nat Rev Drug Discov* 2010;**9**:615-27.

58. Monopoli MP, Aberg C, Salvati A, Dawson KA. Biomolecular coronas provides teh biological indentity of nanosized materials. *Nat Nanotechnol* 2012;**7**:779-86.

59. Jaganathan H, Godin B. Biocompatibility assessment of Si-based nano- and micro-particles. *Adv Drug Deliv Rev* 2012;**64**:1800-19.

60. Choi J, Zhang Q, Reipa V, Wang NS, Stratmeyer ME, Hitchins VM, Goering PL. Comparison of cytotoxic and inflammatory responses of photoluminescent silicon nanoparticles with silicon micron-sized particles in RAW 264.7 macrophages. *J Appl Toxicol* 2009;**29**:52-60.